The Cryosphere Discuss., https://doi.org/10.5194/tc-2017-193
Manuscript under review for journal The Cryosphere
Discussion started: 18 October 2017

The Cryosphere Discussions
Open Access
EGU

Tidal bending of ice shelves as a mechanism for large-scale temporal variations in ice flow

Sebastian, H. R. Rosier[1] and G. Hilmar Gudmundsson[1]
[1]British Antarctic Survey, High Cross, Madingley road, Cambridge, UK
Correspondence to: S. H. R. Rosier (s.rosier@bas.ac.uk)

Abstract. GPS measurements reveal strong modulation of horizontal ice-shelf and ice-stream flow at a variety of tidal frequencies, most notably a fortnightly (M_{sf}) frequency not present in the vertical tides themselves. Current theories largely fail to explain the strength and prevalence of this signal over floating ice shelves. We propose that tidal bending stresses, through the nonlinear rheology of glacier ice, can have a sufficiently large impact on the effective viscosity of ice along its floating margins to give rise to significant and widespread temporal variations in the horizontal velocity of ice shelves. Using full-Stokes viscoelastic modelling, we show that inclusion of tidal bending within the model accounts for much of the observed tidal modulation of ice-shelf flow. Furthermore, our model shows that, in the absence of vertical tidal forcing, the mean flow of the ice shelf is reduced by almost 30 % for the geometry that we consider.

1 Introduction

Ocean tides are known to greatly affect the horizontal flow of both ice shelves and adjoining ice streams, even far upstream of grounding lines (Doake et al., 2002; Brunt et al., 2010; Makinson et al., 2012; Legresy et al., 2004; King et al., 2011; Bindschadler et al., 2003b, a; Anandakrishnan et al., 2003; Alley, 1997; Gudmundsson, 2006; Marsh et al., 2013; Minchew et al., 2016; Rosier et al., 2017). In some cases the ice flow responds at a different frequency to the tidal forcing, for example on the Rutford Ice Stream (RIS) the largest response is at a fortnightly (M_{sf}) frequency (Gudmundsson, 2006). More recent observations have shown that the M_{sf} signal actually increases in strength on the adjoining ice shelf (Minchew et al., 2016; Rosier et al., 2017) and also exists on isolated ice shelves which do not have large ice streams feeding into them (King et al., 2011; Gudmundsson et al., 2017).

The Cryosphere Discuss., https://doi.org/10.5194/tc-2017-193
Manuscript under review for journal The Cryosphere
Discussion started: 18 October 2017

A multitude of mechanisms have been proposed which could lead to a fortnightly modulation in ice flow: a nonlinear basal sliding law (Gudmundsson, 2007, 2011; Rosier et al., 2014), tidal perturbations in subglacial water pressure (Thompson et al., 2014; Rosier et al., 2015), grounding line migration (Rosier et al., 2014) and changes in the effective ice-shelf width (Minchew et al., 2016). Understanding the root cause of the strong and widespread tidal signals observed on ice shelves and ice streams is not done for its own sake but is a means to an end. The periodic and predictable nature of a tidal forcing, together with the complexity of the observed response, means that tides act as a natural experiment with which we can learn about how ice flows and its time-dependant rheological behaviour. The Filchner-Ronne Ice Shelf (FRIS) is a particularly good natural laboratory for gaining these insights because of the considerable tidal range, which can be as large as 9 m (Padman et al., 2002).

Previous modelling studies have focused almost exclusively on tidal modulation of ice-stream flow (Gudmundsson, 2007, 2011; Walker et al., 2012, 2016; Thompson et al., 2014; Rosier et al., 2014, 2015; Rosier and Gudmundsson, 2016; Sergienko et al., 2009), whereas tidal modulation of the flow of ice shelves has received much less attention. This is possibly because it has often been assumed that the M_{sf} signal observed on ice shelves is driven by processes occurring on neighbouring ice streams; indeed these make up the bulk of the proposed mechanisms listed above. Now that new observations show the M_{sf} signal strengthening downstream of GLs (Minchew et al., 2016; Rosier et al., 2017) it has become clear that an alternative mechanism is needed which can generate this signal, independently of anything occurring on grounded ice.

Here, we will show how the observed widespread tidal modulation in ice flow can be generated within ice shelves themselves through tidal flexure. We begin with a description of this simple mechanism, which results directly from the well-known nonlinear flow law of glacier ice and hence does not require an ice stream to act as a source of the observed tidal signals. Then in Sect. 3, using elastic beam theory, we derive a simple mathematical description of this mechanism that yields some insights into its importance for various ice-shelf configurations. Finally in Sect. 6, we present results from a 3-D full-Stokes viscoelastic model of a confined ice shelf, with a similar geometry to the RIS, that incorporates the new mechanism and is capable of replicating many of the observed characteristics of the tidal response of the FRIS. These results will show that this mechanism has important implications for both the time-varying and mean flow of ice shelves subjected to strong vertical ocean tides.

2 Flexural ice-softening mechanism

The Filchner-Ronne, Larsen and to a lesser extent Ross Ice Shelves are situated in tidally energetic regions, and thereby subjected to large vertical motion at tidal frequencies. By far the largest tidal amplitudes are in the Weddell Sea region, particularly at the grounding line of large ice streams such

The Cryosphere Discuss., https://doi.org/10.5194/tc-2017-193
Manuscript under review for journal The Cryosphere
Discussion started: 18 October 2017

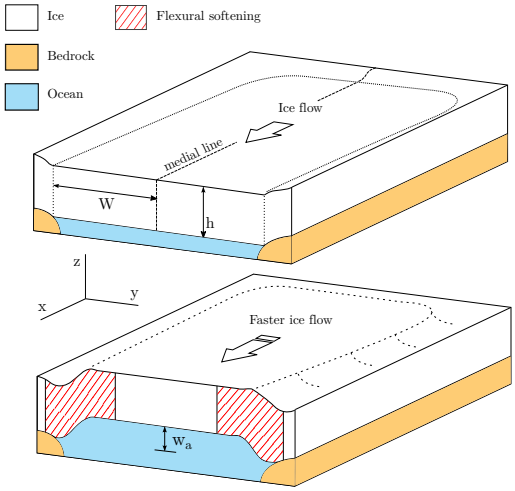

Figure 1. Schematic showing the flexural ice-softening mechanism for a confined shelf, together with the geometry of the problem described in Sect. 3. The top panel shows the situation with no tidal uplift and the bottom panel shows how ice flow is enhanced as ice is softened in the shear margins due to flexural stresses generated by a vertical tidal motion (w_a).

as Rutford and Evans (Padman et al., 2002). In the grounding zone (a band along the grounding lines that extends several kilometers into the main shelf) the ice bends to accommodate these large vertical tidal motions. This bending generates longitudinal and shear stresses within the ice which contribute to the effective stress and are strongest near the grounding line during high and low tide. Since ice is a non-Newtonian shear thinning fluid its effective viscosity will be altered by these tidal stresses. Specifically, at high and low tide the effective ice viscosity will be reduced compared to the situation with no vertical tidal motion. This effect, which we will call 'flexural ice-softening', leads to an increase in ice velocity during high and low tide. This is simply a consequence of the nonlinearity of Glen's flow law.

Since it is the magnitude of stresses and not their sign that contributes to the effective viscosity, there is no difference in the flexural ice-softening effect between high and low tide. The only time that the effective viscosity of an ice shelf subjected to large tides will increase to that of an ice shelf without tides is when the vertical deflection is small, i.e. between high and low tide or during neap tides. As a consequence there are two other important repercussions for the ice-shelf flow that arise from this mechanism, aside from the direct increase in velocity at high and low tide. Firstly, the mean flow of an ice shelf is greater in the presence of large tides because, even at its slowest, it will be flowing equally as fast as an ice shelf without tides. Secondly, because the change in velocity (due to effective softening) during spring tide is much larger than during neap tide, the ice shelf flow

The Cryosphere Discuss., https://doi.org/10.5194/tc-2017-193
Manuscript under review for journal The Cryosphere
Discussion started: 18 October 2017

will be modulated at an M_{sf} period (provided the rheology is nonlinear, as is the case for glacier ice). Since many large ice shelves are confined on three sides by grounded ice, the bending stresses are generated along their entire length. This mechanism could therefore explain how the M_{sf} signal increases in strength downstream of ice stream grounding lines, as evidenced by recent GPS and satellite observations (Minchew et al., 2016; Rosier et al., 2017). A schematic showing how vertical tidal motion can lead to a reduction in effective viscosity of ice shelf shear margins is shown in Fig. 1.

3 Analytical solution for flexural ice-softening

Elastic beam theory provides a useful starting point for evaluating the magnitude of these tidal bending stresses on an ice shelf and their impact on its effective viscosity. We start from a simple confined ice shelf whose geometry is invariant across flow (in the y direction) and with a constant thickness gradient in the down-flow x direction. The ice shelf is symmetrical about the centerline, which is distance W from the two sidewalls at $y = 0$ and $y = 2W$ (Fig. 1). For this analytical solution we assume that the portion of the ice shelf that we investigate is sufficiently far from the GL that the only bending occurs across-flow. The situation near the main GL of a narrow confined shelf will be a complex combination of along and across-flow stresses that we shall ignore for now. Deviatoric stresses are defined as

$$\tau_{ij} = \sigma_{ij} - \delta_{ij}\sigma_{kk}/3 \tag{1}$$

where σ_{ij} are the components of the cauchy stress tensor, δ_{ij} is the Kronecker delta and $p = -\sigma_{kk}/3$ is the isotropic pressure. We use the comma to denote partial derivatives and the summation convention, in line with standard tensor notation.

We immediately make the simplifying assumptions (motivated by full-Stokes calculations presented below) that $\tau_{xx} = \tau_{xz} = 0$, hence $\tau_{yy} = -\tau_{zz}$, $\sigma_{zz} = -p - \tau_{yy}$ and $\sigma_{xx} = -p$. Furthermore, we assume that the only important contributions to τ_{yy} and τ_{yz} are due to tidal bending. The Stokes flow equations in x and z reduce to the following form:

$$-\partial_x p + \partial_y \tau_{xy} = 0 \tag{2a}$$

$$\partial_y \tau_{yz} + \partial_z \sigma_{zz} = \rho g \tag{2b}$$

Note that in this system σ_{zz} is not cryostatic, unlike in the shallow shelf and shallow ice approximations. We are interested in finding an expression for the across-flow variation in downstream velocity, $u(y)$, for which we need an expression for τ_{xy}. As we show in appendix A, τ_{xy} is essentially independent of the tidal stresses (as well as x and z) and can be approximated by

$$\tau_{xy} = F_d h(W - y), \tag{3}$$

where $F_d = \rho g \partial_x s$.

The Cryosphere Discuss., https://doi.org/10.5194/tc-2017-193
Manuscript under review for journal The Cryosphere
Discussion started: 18 October 2017

Linear elastic beam theory gives us an expression for the elastic stresses that will arise due to tidal bending (Robin, 1958). Although strictly derived for an infinitely long ice shelf, we show in appendix B that the equations in Robin (1958) provide a good approximation for the geometry that we are interested in. The two contributing stresses, related to the bending moment and its derivative, are the across-flow longitudinal bending stress:

$$\tau_{yy} = \frac{-6 w_a \rho_w g z}{h^3 \lambda^2} e^{-\lambda y} \left[\cos(\lambda y) - \sin(\lambda y)\right] \tag{4}$$

and the across-flow shear bending stress:

$$\tau_{yz} = \frac{6 \rho_w g w_a}{h^3 \lambda} e^{-\lambda y} \cos(\lambda y) \left[\frac{h^2}{4} - z^2\right], \tag{5}$$

where

$$\lambda^4 = \frac{3 \rho_w g (1-\mu^2)}{E h^3}, \tag{6}$$

w_a is the vertical tidal motion, E is the Young's modulus of ice, μ is the Poisson's ratio and ρ_w is the density of seawater. The vertical coordinate, z, is defined as the vertical distance above the neutral axis of the ice shelf, which we assume to be halfway through its thickness.

At this stage we employ a nonlinear Maxwell rheological model to find the resultant ice velocities. With this viscoelastic model the viscous and elastic stresses are equal and the total strain is the sum of the strain in the two components. In this way, we can express the horizontal shear strain rate as

$$\dot{e}_{xy} = 2A \tau_E^{n-1} \tau_{xy} + \frac{1}{G} \dot{\tau}_{xy} \tag{7}$$

where

$$G = \frac{E}{2(1+\mu)} \tag{8}$$

and, based on the assumptions given above,

$$\tau_E \approx \sqrt{\tau_{yy}^2 + \tau_{xy}^2 + \tau_{yz}^2}. \tag{9}$$

Motivated both by our findings in the appendix that $\dot{\tau}_{xy} \approx 0$, and by the fact that this elastic term can only ever yield a linear response to the tidal forcing, we discard it and focus only on the nonlinear viscous response. We are concentrating on the nonlinear response because only this can explain modulation of ice-shelf flow at an M_{sf} frequency, given that the M_{sf} constituent is absent in the vertical tidal forcing.

By assuming that $n = 3$, we can separate the velocity into unperturbed and time-varying components. Integrating along y then gives the depth averaged velocity $\overline{u}$ as

$$\overline{u}(y,t) = \frac{2A}{h} \left(\overbrace{\int_0^y \overline{\tau_{xy}}^3 dy}^{u_0} + \overbrace{\int_0^y \overline{\tau_{xy}} \int_b^s \tau_{yy}^2 \, dz dy}^{u_{\mathrm{long}}} + \overbrace{\int_0^y \overline{\tau_{xy}} \int_b^s \tau_{yz}^2 \, dz dy}^{u_{\mathrm{shear}}} \right) \tag{10}$$

The Cryosphere Discuss., https://doi.org/10.5194/tc-2017-193
Manuscript under review for journal The Cryosphere
Discussion started: 18 October 2017

where $\overline{\tau_{xy}} = \tau_{xy}/h$. We have split this into the three components, denoted as the unperturbed (u_0), long(itudinal) bending stress and shear bending stress contributions to ice flow. Evaluating the integrals for each term and neglecting the overbar since everything is now depth averaged yields:

$$u_{\text{long}} = \frac{3AF_d(\rho_w g w_a)^2}{2h^4\lambda^6}\left[e^{-\gamma}\left(1-2\xi+\xi\sin(\gamma)+\cos(\gamma)\left[\xi-\frac{1}{2}\right]\right)+\lambda W-\frac{1}{2}\right] \tag{11}$$

where $\xi = \lambda W - \frac{\gamma}{2}$ and $\gamma = 2\lambda y$,

$$u_{\text{shear}} = \frac{3AF_d(\rho_w g w_a)^2}{10h^2\lambda^4}\left[e^{-\gamma}\left(1-2\xi-\xi\cos(\gamma)+\sin(\gamma)\left[\xi-\frac{1}{2}\right]\right)+3\lambda W-1\right] \tag{12}$$

and

$$u_0 = \frac{1}{2}AF_d^3\left(W^4-(W-y)^4\right). \tag{13}$$

The shear and longitudinal components can be combined, such that the total (time-varying) velocity $u = u_0 + \Delta u$. Along the centerline at $y = W$, the change in velocity due to tides (Δu) is

$$\Delta u = w_a^2 B, \tag{14}$$

where

$$B = \frac{3AF_d\rho_w^2 g^2}{2h^2\lambda^2}\left(e^{-\gamma}\left[\frac{1}{5}-\frac{\sin(\gamma)}{10}+\frac{1}{h^2\lambda^2}-\frac{\cos(\gamma)}{h^2\lambda^2}\right]+\frac{3\lambda W}{5}-\frac{1}{3}+\frac{W}{h^2\lambda}-\frac{1}{2h^2\lambda^2}\right) \tag{15}$$

To illustrate the consequences of a typical tidal action for the ice-shelf flow, we assume that the time-varying sea level $w_a(t)$ can be written as the sum of two cosines of amplitude a_{M_2} and a_{S_2} and angular frequency ω_{M_2} and ω_{S_2}, i.e.

$$w_a(t) = a_{M_2}\cos(\omega_{M_2}t) + a_{S_2}\cos(\omega_{S_2}t). \tag{16}$$

These two cosines represent the principal lunar (M_2) and solar (S_2) semidiurnal tides, which dominate in the area of interest. Crucially, because the velocity is a function of tidal deflection squared, new frequencies emerge which, if we assume it takes the form of Eq. 16, expands as follows:

$$w_a^2 = \frac{a_{M_2}^2+a_{S_2}^2}{2} + \overbrace{\frac{a_{M_2}^2}{4}\cos(2\omega_{M_2}t)}^{M_4} + \overbrace{\frac{a_{S_2}^2}{4}\cos(2\omega_{S_2}t)}^{\text{S4}} + \overbrace{\frac{a_{M_2}a_{S_2}}{2}\cos(\omega_{M_{S4}}t)}^{MS_4} + \overbrace{\frac{a_{M_2}a_{S_2}}{2}\cos(\omega_{M_{sf}}t)}^{M_{\text{sf}}}, \tag{17}$$

where $\omega_{M_{sf}} = \omega_{S_2} - \omega_{M_2}$ and $\omega_{M_{S4}} = \omega_{M_2} + \omega_{S_2}$. The four emergent frequencies that we expect to see are labelled according to their respective tidal constituent names. Depending on the relative size of the M_2 and S_2 vertical tidal forcing, different frequencies will dominate in the horizontal ice flow response. In the case of the Filchner-Ronne Ice Streams, the amplitude of the S_2 constituent is

The Cryosphere Discuss., https://doi.org/10.5194/tc-2017-193
Manuscript under review for journal The Cryosphere
Discussion started: 18 October 2017

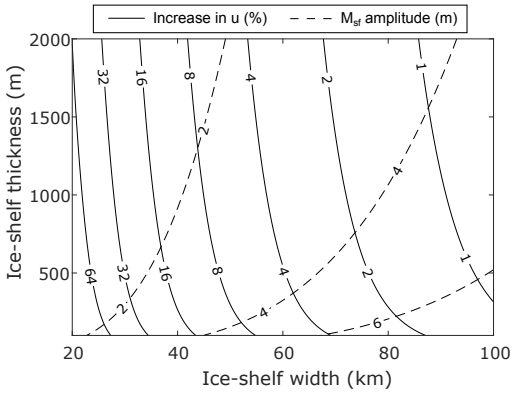

Figure 2. Contour plot of ice-shelf speed up due to tides, as a percent of the baseline speed, predicted by the analytical solution in Eq. 18. Speed-up is predicted along the ice shelf medial line using parameter values given in table 3. Also shown are contours of the amplitude of the M_{sf} signal in ice-shelf displacements (dashed contours).

typically about half that of the M_2 constituent. As a result, the S_4 frequency will be much smaller than the other three. In terms of velocities, the amplitudes of the M_{sf} and MS_4 components will be equal, and larger than the M_4 component as long as $a_{S_2} > a_{M_2}/2$. We explore this in more detail later.

Several useful results are now easily obtained with Eqs. 17 and 14, for example the amplitude of the M_{sf} component in ice-shelf velocity is simply $(Ba_{M_2}a_{S_2})/2$. Integrating with time gives an expression for displacements, which are more readily measured with in-situ GPS. Once again, the amplitude of the M_{sf} component in displacements in this case becomes $(Ba_{M_2}a_{S_2})/2(\omega_{S_2} - \omega_{M_2})$. Even more interesting is the result of the first term of Eq. 17, which acts to increase the time-averaged ice-shelf velocity (u_{mean}). The size of this effect, which we call the n_{shift} is given by

$$n_{\text{shift}} = \frac{B(a_{S_2}^2 + a_{M_2}^2)}{2}, \tag{18}$$

such that $u_{\text{mean}} = u_0 + n_{\text{shift}}$. Interestingly, within this framework all tidal energy at the original (vertical) semidiurnal forcing frequencies disappears. In reality linear elastic effects and changes in damming stresses would be expected to produce some response at these frequencies. Note that from Eq. 10 onwards these results have been derived under the assumption that $n = 3$. For $n = 1$ bending stresses have no impact on the ice-shelf viscosity and so the M_{sf} flow-modulation and n_{shift} would be identically equal to zero.

Using the simple set of equations outlined above we can easily explore the parameter space to see how the strength of the tidal response changes. Of particular interest is how the n_{shift} leads to an increase in the mean speed of the ice shelf. In Fig. 2 we show speed-up along the ice shelf medial line (solid black contour) as a percent of the baseline speed with no tides, i.e. u_{mean}/u_0 (the parameters

The Cryosphere Discuss., https://doi.org/10.5194/tc-2017-193
Manuscript under review for journal The Cryosphere
Discussion started: 18 October 2017

Table 1. Choice of parameters used in Eq. 18 to produce Fig. 2.

Parameter	Value	Unit
n	3	-
a_{M_2}	1	m
a_{S_2}	1	m
ρ	910	$\mathrm{kg\,m^{-3}}$
ρ_w	1030	$\mathrm{kg\,m^{-3}}$
g	9.81	$\mathrm{m\,s^{-2}}$
μ	0.3	-
E	800	kPa
$\partial_x s$	5e-4	-

chosen are shown in table 3). This shows that, for a given tidal amplitude, the n_{shift} effect will be most strongly felt on a narrow, thin ice shelf. Conversely, the amplitude of the M_{sf} signal in ice shelf displacements (dashed contour) is strongest for wide, thick ice shelves. The apparent discrepancy is because, with all other parameters held constant, a wider ice shelf will flow much faster and so the increase in speed as a percent of the baseline is much less.

Note that we use a different value of E in this analytical solution than for our full-Stokes model. In reality, the Young's Modulus of ice is frequency dependant and using the instantaneous Young's modulus of 9 GPa (suggested by laboratory experiments) will result in bending stresses that are far too large. Instead, we treat this value as a tuning parameter and pick a value of E that best matches our modelled bending stresses, which turns out to be 800 kPa.

4 Full-Stokes Model Description

In order to explore the idea of flexural ice-softening in more detail, we undertook modelling experiments on an idealised ice stream/shelf domain using the commercial finite element software MSC.Marc, which has been used extensively in the past to explore the tidal response of ice streams (Gudmundsson, 2011; Rosier et al., 2014, 2015; Rosier and Gudmundsson, 2016). The idealised ice stream is 28km wide (to match the approximate average width of the RIS) and consists of a 150 km floating shelf and 80 km grounded ice (Fig. 3). Although data now exists showing tidal modulation on other ice streams, the RIS lends itself well to an idealised study of this kind because of its relatively simple geometry and because its flow has remained largely unchanged over the measurement period (Gudmundsson and Jenkins, 2009). Surface and bed slopes of the ice stream and ice-shelf portions of the model are approximate averages of the slopes found on RIS, and ice thickness at the downstream limit of the domain is 1420 m. The model is run forward in time for 60 days in order

The Cryosphere Discuss., https://doi.org/10.5194/tc-2017-193
Manuscript under review for journal The Cryosphere
Discussion started: 18 October 2017

to resolve the M_{sf} signal. The grounding line position is fixed and cannot migrate at tidal frequencies, since our focus is only on the effects of tidal bending stresses. We investigate several test cases (Sect. 5), some of which require a slightly different model set up, which we describe in the relevant sections.

4.1 Field Equations

The full-Stokes solver MSC.Marc uses the finite element method in a Lagrangian frame of reference to solve the field equations:

$$\frac{D\rho}{Dt} + \rho v_{i,i} = 0, \tag{19}$$

$$\sigma_{ij,j} + f_i = 0, \tag{20}$$

$$\sigma_{ij} - \sigma_{ji} = 0, \tag{21}$$

representing conservation of mass, linear momentum and angular momentum, respectively. In the above equations, D/Dt is the material time derivative, v_i are the components of velocity, σ_{ij} are the components of the stress tensor, ρ is the ice density and f_i are the components of the gravity force.

We use a nonlinear Maxwell viscoelastic rheology in a slightly modified form to Eq. 7, which can be written as

$$\dot{e}_{ij} = \frac{1}{2G}\overset{\triangledown}{\tau}_{ij} + A\tau_E^{n-1}\tau_{ij}, \tag{22}$$

where the full stress tensor contributes to the effective stress, i.e.

$$\tau_E = \sqrt{\tau_{ij}\tau_{ji}/2} \tag{23}$$

and the superscript $\triangledown$ denotes the upper-convected time derivative:

$$\overset{\triangledown}{\tau}_{ij} = \frac{D}{Dt}\tau_{ij} - \frac{\partial v_i}{\partial x_k}\tau_{kj} - \frac{\partial v_j}{\partial x_k}\tau_{ik} \tag{24}$$

(Christensen, 1982). We use the same rheological parameters as in Gudmundsson (2011), which are found to replicate the behaviour of the more complex Burgers model at tidal frequences, i.e. $E = 4.8$GPa and $\mu = 0.41$.

4.2 Boundary Conditions

At the downstream limit of the domain we prescribe the ice shelf stresses:

$$\sigma_{xx} = -\rho g(s-z) + \frac{\rho g h}{2}\left(1 - \frac{\rho}{\rho_w}\right) - p_b \tag{25}$$

The Cryosphere Discuss., https://doi.org/10.5194/tc-2017-193
Manuscript under review for journal The Cryosphere
Discussion started: 18 October 2017

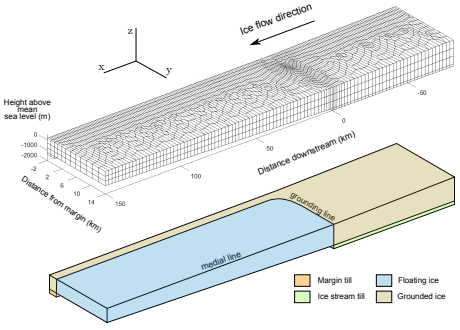

Figure 3. Finite element mesh used in the full-Stokes viscoelastic model (Sect. 4). Note that x and y horizontal scales have been reduced by factor 10 and 2 respectively.

and

$$\tau_{xz} = -\rho g z \left(\frac{\partial s}{\partial x} - \frac{1}{2} \frac{\partial h}{\partial x} \left(1 - \frac{\rho}{\rho_w} \right) \right) \tag{26}$$

where p_b is a buttressing term. A value of 250kPa was chosen for p_b, in order to reproduce ice shelf velocities similar to those observed at the outlet of the RIS. At the upstream boundary we apply the cryostatic pressure $\sigma_{xx} = \rho_i g(s - z)$.

The ocean pressure normal to the ice ocean interface (p_w) is applied as an elastic foundation:

$$p_w = -\rho_w g(z - w_a(t)) \tag{27}$$

where z is the depth below sea level and $w_a(t)$ is the time varying vertical tidal motion (Sect. 5.1).

Upstream of the grounding line, along the ice-bed interface, we use a Weertman style sliding law of the form

$$u = c\tau_b^m \tag{28}$$

where c is basal slipperiness, τ_b is the along-bed tangential component of the basal traction and m is a stress exponent. In all of our experiments we use a nonlinear sliding law with $m = 3$. Similarly, slipperiness values beneath the ice stream are kept fixed in all experiments to a value that approximately matches the mean flow velocity of the RIS. Beneath the margin, slipperiness is made several orders of magnitude smaller to restrict ice flow in this portion of the model.

We treat one side of the model ice stream as the medial line, since the problem is symmetrical ($\partial_y h = 0$), meaning we only need to model half of the ice stream with no lateral flow as the appropriate BC. The other side is treated as a grounded sidewall with no-slip, such that $u = v = w = 0$ (referred to hereafter as the clamped BC). In one of the experiments (**n3xy**) the constraint on vertical velocity is removed, as explained in Sect. 5.

The Cryosphere Discuss., https://doi.org/10.5194/tc-2017-193
Manuscript under review for journal The Cryosphere
Discussion started: 18 October 2017

4.3 Element Discretization

The model uses 20-node isoparametric hexahedral (brick) elements with a 27-point Gaussian integration scheme. These quadratic elements allow accurate representation of stresses and strains with much fewer numbers of elements than would typically be used. Element size varies from a maximum horizontal dimension of ∼2km to a minimum of ∼300m around the grounding line and in the shear margins. The finite element mesh is unstructured, with a GL that curves to avoid an unnatural grounding zone corner. The ice is 3 elements thick vertically, resulting in 9 integration points through its depth. The model mesh is shown in Fig. 3.

5 Model Experiments

We conduct three simple model experiments to investigate the effects of flexural ice-softening within our model.

n3xyz In the first experiment, denoted **n3xyz**, we run the model with nonlinear ice rheology and sidewalls clamped in x,y and z. This is designed to simulate the 'Rutford' case whereby the margins are essentially stagnant and flexure occurs all along the GL, both where the main body of the ice stream meets the ocean and downstream of this point along the sides. In order to approximately match the observed 1m/d flow velocities of the floating portion of RIS we adjust the ice rate factor (A) uniformly.

n3xy For the second experiment, denoted **n3xy**, we run the model as in **n3xyz** but the sidewalls downstream of the GL are not clamped vertically (z direction). With this setup there is no bending along the sidewalls downstream of the GL, so flexural stresses are only generated in the grounding zone around $x = 0$. This experiment is akin to a fast flowing ice-shelf bounded by stagnant floating ice, as can be found on the floating portion of some fast flowing outlet glaciers.

n1xyz The third experiment, denoted **n1xyz**, uses exactly the same setup and boundary conditions as in **n3xyz** except that ice rheology is made linear, such that $n = 1$ in Eq. 22. In this situation the ice is still bending all along the GL but the stresses setup by this bending have no impact on the ice's effective viscosity. As such, it is not a 'realistic' situation (since ice is known to have a nonlinear rheology) but serves to emphasise that this nonlinearity is the important one at play in our model. In order to produce sensible ice-shelf velocities, the rate factor A is adjusted uniformly in this experiment so that the background flow-speed (denoted u_{mean} in the previous analysis) is approximately the same.

The Cryosphere Discuss., https://doi.org/10.5194/tc-2017-193
Manuscript under review for journal The Cryosphere
Discussion started: 18 October 2017

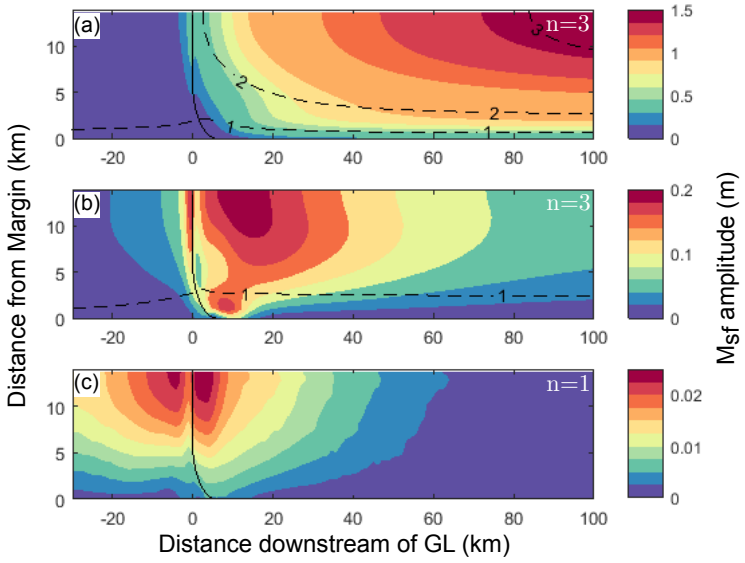

Figure 4. M_{sf} amplitude calculated with the full-Stokes viscoelastic model for the three experiments described in Secion 5. Panel a shows experiment **n3xyz**, i.e. the standard case with $n = 3$ and bending all along the sidewall boundary. Panel b shows experiment **n3xy** in which the ice only bends at the $x = 0$ GL. Panel c shows the **n1xyz** experiment, for which $n = 1$ but with the same BCs as panel a. Dashed black lines in the top two panels are contours of downstream velocity and solid black lines show the GL position. Note the differences in colour scale between each panel.

5.1 Tidal Forcing

The time-varying vertical tidal forcing is implemented through the ocean foundation BC (Eq. 27. For all the experiments described above the model is forced with the principal semidiurnal (M_2 , S_2) and diurnal (O_1 , K_1) tidal constituents, i.e. the four tidal constituents which are generally largest beneath the FRIS. Their amplitudes are derived from GPS measurements of vertical ice-shelf motion 20km downstream from RIS GL (Gudmundsson, 2006). The tidal forcing is kept intentionally simple to avoid complicating any interpretation of our full-Stokes model results.

6 Model Results

We now present results from our viscoelastic 3D full-Stokes model of an idealised ice-stream/shelf system. We begin by examining the modelled response at M_{sf} frequency, since previous models do not reproduce observations of this nonlinear effect on floating ice shelves. M_{sf} amplitude in ice shelf displacements is shown in plan view for the three experiments in Fig. 4. For the **n3xyz** experiment, which can be thought of as the typical situation for a confined ice shelf subjected to large vertical

The Cryosphere Discuss., https://doi.org/10.5194/tc-2017-193
Manuscript under review for journal The Cryosphere
Discussion started: 18 October 2017

tides, M_{sf} amplitude increases continuously downstream of the GL (Fig. 4a). In the across flow (y) direction the amplitude increases towards the medial line. Also shown are contours of ice-shelf velocity (u), which increase from 1 m/d upstream of the GL to more than 3 m/d on the shelf.

In the **n3xy** experiment the only change is to remove the vertical clamp BC acting along the sidewall of the floating portion of the model. In this situation the M_{sf} amplitude decays away from the GL and is reduced to almost zero far downstream (Fig. 4b). The change in sidewall BC also leads to a slightly different pattern in M_{sf} amplitude across the GL. Ice-velocities on the floating shelf are lower than in the **n3xyz** experiment, and the 1 m/d contour is located further from the margin.

For the third experiment, denoted **n1xyz**, (Fig. 4c), where ice rheology is linear but ice still bends all along the margins, the M_{sf} response is even more localised to the GL region and the amplitude is far lower than the other two experiments.

Running the standard **n3xyz** experiment with and without tides reveals how the mean ice-shelf flow is affected by tidal bending stresses. Averaging over the entire floating portion of the shelf, mean velocity is increased by $\sim$35% when the experiment is run with a vertical tidal forcing equivalent to that experienced near the RIS GL, as against with no tidal forcing.

Other tidal frequencies that emerge from the frequency doubling (17), such as MS_4 , show very similar spatial patterns to the M_{sf} responses shown in Fig. 4, except that they are completely absent for the **n1xyz** experiment.

To explore the role of flexural stresses in more detail we plot across-flow profiles for each component of the deviatoric stress tensor (Fig. 6). Stresses are taken from the **n3xyz** experiment at $x = 100$ km, to avoid the 2-D bending stresses at $x = 0$, and for a positive vertical tidal deflection of 2 m. The stress is scaled by the depth-averaged horizontal shear stress at the margin $\rho g W \partial_x s$, as predicted by the analysis in Sect. 3 (for the ice-shelf surface slope in the model of 5.4×10^{-4} the stress scale is 67.5 kPa). Distance from the margin is scaled by the ice-shelf half-width ($W =$ 14 km).

Surface and bed longitudinal bending stress are equal but opposite in sign and so we plot the depth average of their absolute values. This is more relevant for our purposes, since it is the absolute amplitudes of these stresses, and not their signs, that impact the effective stress. For $w_a = 2$ the longitudinal flexural stresses (τ_{yy}) reach $\sim$ 40kPa and contributes a large portion of the total effective stress. Flexural stresses reduce to almost zero at a distance of $\pi/4\lambda$ from the margin but then increase with opposite sign and once again contribute a large proportion of the total effective stress up to a distance of $\sim$ 12 km. Shear bending stresses (τ_{yz}) are of a similar size at the margin but decay more rapidly towards the centerline. Note that, since λ is a function of ice thickness, the location of the bending stress minima will shift as the thickness changes.

At this stage we can briefly evaluate the validity of the assumptions made in Sect. 3. A linear variation in τ_{xy} matches very closely with the full-Stokes model results. The assumption that $\tau_{yy} \approx -\tau_{zz}$ is a good one near the margin but breaks down towards the centerline where τ_{xx} becomes

The Cryosphere Discuss., https://doi.org/10.5194/tc-2017-193
Manuscript under review for journal The Cryosphere
Discussion started: 18 October 2017

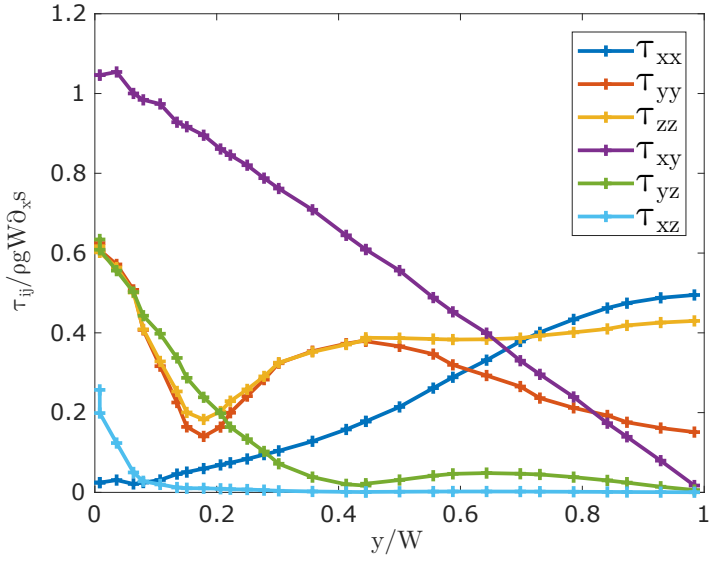

Figure 5. Across-flow transects of depth averaged non-dimensional stress from the full-Stokes viscoelastic model (Sect. 4) for experiment **n3xyz**. Profiles are taken 100 km downstream of the GL at high tide ($w_a = 2$ m). The stress scale is given by $\tau_{ij}/\rho g W \partial_x s$ and the length scale by y/W.

important. Finally, the vertical shear stress (τ_{xz}) is small everywhere, although shearing of grounded ice in the sidewalls does result in some stress on the neighbouring shelf.

7 Discussion

The analysis of Sect. 3, together with full-Stokes viscoelastic modelling, both suggest that flexural ice-softening could play an important role in the generation of the M_{sf} signal that is readily observed across the entire FRIS region (Rosier et al., 2017). Flexural stresses due to vertical tidal motion can generate a fortnightly modulation in ice flow along any GL based only on the fact that ice is non-Newtonian. This mechanism is felt most strongly for a confined ice shelf, where bending occurs in the margins along the entire length of the shelf. New observations of the M_{sf} signal reveal that it is generally larger on the floating ice shelf and tends to increase in amplitude towards the ice front (Minchew et al., 2016; Rosier et al., 2017). Our modelling work shows that flexural ice-softening can replicate this amplification of the M_{sf} signal downstream of ice stream GLs. Furthermore, these tidal bending stresses will lead to a net speed-up of the ice shelf.

Another mechanism has previously been proposed by Minchew et al. (2016) to explain the M_{sf} amplification on ice shelves. In Minchew et al. (2016), the shelf width is defined as the distance be-

The Cryosphere Discuss., https://doi.org/10.5194/tc-2017-193
Manuscript under review for journal The Cryosphere
Discussion started: 18 October 2017

tween the two maxima of lateral shear strain rate and changes in this metric are interpreted as being caused by grounding line migration. An alternative explanation is that flexural ice-softening in the shear margins leads to a steepening of the across-flow velocity profile at the boundary, thereby shifting the apparent margin as defined above. Calculating lateral shear strain rate 100 km downstream of the **n3xyz** simulation shows that each peak can shift by ∼500 m over a tidal cycle, leading to an apparent widening of 1 km even though there is no grounding line migration in the model. Alternative evidence of GL migration does exist in other parts of the FRIS (Brunt et al., 2011) and this mechanism could be locally important, however, it seems unlikely that it could explain the pervasiveness of the M_{sf} signal across the entire shelf, since it is so reliant on local bedrock topography.

The flexural ice-softening mechanism produces a frequency doubling in the response of the ice shelf; since the marginal ice will be softest at both high and low tide. This is also evident in the analysis of Sect. 3, which reveals that ice velocity will be modulated at M_4 and MS_4 frequencies in addition to the M_{sf} frequency which dominates the displacements. We performed a tidal analysis on modelled displacement and velocity at the ice stream medial line, 100km downstream from the GL and ignoring constituents with a low signal to noise ratio (Fig. 6). Surface horizontal displacements show a dominantly M_{sf} response, with almost no clear response at other frequencies (Fig. 6a). In the horizontal ice velocity (Fig. 6b) the M_4 and MS_4 frequencies emerge, with similar amplitudes to the M_{sf} in agreement to Eq. 17. Other nonlinear frequencies such as M_{f} , arising from interaction of the two diurnal tidal constituents, should be present but would only be resolvable with much longer model run times.

The change in dominant frequency between ice-shelf velocities and displacements is predicted by the analysis of Sect. 3. Since displacements are integrated velocities the constituent terms of Eq. 17 are divided by their frequencies, which greatly amplifies longer period constituents such as M_{sf} and visa versa for shorter frequencies. These results suggest that our best chance at finding evidence of the flexural ice-softening mechanism would be to look at short-term velocity fluctuations of floating ice. In contrast to other proposed mechanisms that could potentially generate the M_{sf} signal on a floating ice shelf, this new mechanism is the only one that would lead to diagnostic MS_4 and M_4 modulation of ice shelf velocities.

Most of our observations of the short-term velocity fluctuations on floating ice come from GPS units. Tidal analysis of these records is typically done on their measured displacements, rather than the much noisier velocities calculated from the time derivative of their measured position. By first fitting a tidal model to GPS measurements of horizontal ice flow downstream of the RIS, and then calculating the velocity from this smooth field, we can get a better velocity signal with which to do further analysis.

A convenient measure of the importance of each tidal constituent is the percent energy (PE) (Codiga and Rear, 2004). Tidal analysis with Utide (Codiga, 2011) of the measured horizontal ice displacements 20 km downstream of RIS GL show that the M_{sf} signal dominates with 87% of PE,

The Cryosphere Discuss., https://doi.org/10.5194/tc-2017-193
Manuscript under review for journal The Cryosphere
Discussion started: 18 October 2017

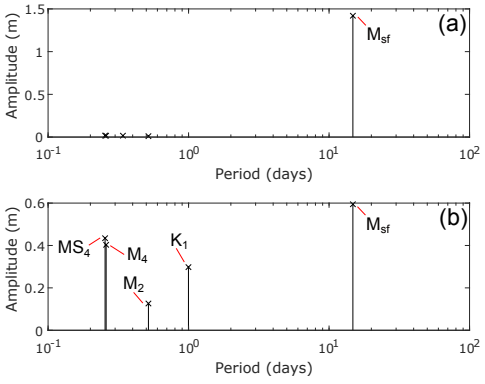

Figure 6. Tidal analysis of horizontal displacement (panel a) and velocity (panel b) from the full-Stokes model, taken at the medial line, 100km downstream of the GL. Notable tidal constituents are labelled with their respective names.

followed by the diurnal and semidiurnal tidal constituents. Analysis of the velocites, calculated as described above, reveals that the two largest constituents are M_4 and MS_4 with 21% and 13% of PE, respectively. Given that no other proposed mechanism would produce these high frequency constituents, this is strong evidence that flexural ice-softening is the dominant process producing the M_{sf} signal on the floating portion of RIS.

As has already been mentioned, a multitude of nonlinear mechanisms have been put forward to explain the observed M_{sf} modulation of ice flow due to tides. We do not include most of these mechanisms in our model and choose instead to focus on the impact of flexural ice-softening in isolation. All of the proposed nonlinear mechanisms could potentially play some role in generation of the M_{sf} signal, depending on local conditions, although most of them are only valid on grounded ice. That being said, the simplicity of the mechanism and the ease with which it explains many observations of tidal modulation in ice-shelf flow would suggest that this might be the primary mechanism at play.

In all our full-Stokes model experiments the M_{sf} signal decays rapidly upstream of the grounding line, contrary to observations which show the signal persists up to ∼80 km upstream of the Rutford, Evans and Foundation Ice Stream GLs (Gudmundsson, 2006; Minchew et al., 2016; Rosier et al., 2017). Other mechanisms have been suggested which could promote propagation of this signal far upstream, for example weakened margins or tidal pressurisation of the subglacial drainage system. Since our focus is on the ice-shelf we do not include any of these mechanisms in this model.

To this day there remains some debate about the correct value for the ice rheological exponent n and whether it might vary spatially (Cuffey and Paterson, 2010, and references therein), although this is often conveniently ignored in modelling studies. Since the amplitude of the M_{sf} signal on the ice

The Cryosphere Discuss., https://doi.org/10.5194/tc-2017-193
Manuscript under review for journal The Cryosphere
Discussion started: 18 October 2017

shelf is highly sensitive to the value of n, further modelling of this effect might help to provide new insights into ice rheology. For example, it might be that the observed spatial pattern and magnitude of the M_{sf} effect on the shelf downstream of RIS can only be reproduced for certain choices of n.

8 Conclusions

We present results from both analytical and full-Stokes models, which show that tidal bending stresses in ice-shelf margins can give rise to large scale temporal variations in ice flow. The non-linear rheology of ice means that, as an ice-shelf bends to accomodate vertical tidal motion, stresses generated in the grounding zone reduce the effective viscosity of ice. This leads to modulation of ice-shelf velocity at a number of frequencies, including the M_{sf} frequency which is readily observed on many Antarctic ice shelves (King et al., 2011; Minchew et al., 2016; Gudmundsson et al., 2017; Rosier et al., 2017). In addition, the nonlinear response changes the mean flow of the ice shelf when it is subjected to vertical tidal motion.

This mechanism relies only on the nonlinear rheology of ice and can explain many recent GPS and satellite observations of tidal effects on ice-shelf flow. Unlike previous mechanisms, it leads to a frequency doubling effect which is potentially diagnosable from careful measurement of ice-shelf velocity with high temporaly resolution and accuracy. Tentative analysis of GPS measurements from the floating portion of RIS suggest that these characteristic frequencies can be seen in existing data.

The bending stresses investigated in this study are typically ignored and difficult to incorporate into large-scale ice-sheet models, however this work shows that these stresses have a role to play in the overall flow-regime. Full-Stokes modelling of a tidally energetic region such as the FRIS would lead to further insights into the importance of this mechanism, its relevance for ice flow models and possibly even ice rheology.

Appendix A: Derivation of across-flow shear stress

We start from the simplified z-momentum given in Eq. 2b, together with expressions for the bending stresses τ_{yy} and τ_{yz} (Eqs. 4 and 5 respectively). Applying the surface boundary condition $\sigma\hat{\mathbf{n}} = 0$ we find that

$$-\partial_y s\,\tau_{yz}(s) + \sigma_{zz}(s) = 0. \tag{A1}$$

Since $\tau_{yz} = 0$ at the surface, this reveals that $\sigma_{zz}(s) = 0$.

Using this result and integrating the z-momentum (Eq. 2b) from the surface to arbitrary depth z we arrive at an expression for $p(x, y, z, t)$:

$$p = \rho g(s - z) - \tau_{yy}(z) - \int_z^s \partial_y \tau_{yz}\, dz. \tag{A2}$$

The Cryosphere Discuss., https://doi.org/10.5194/tc-2017-193
Manuscript under review for journal The Cryosphere
Discussion started: 18 October 2017

Inserting this into the x-momentum of Eq. 2a gives

$$\partial_y \tau_{xy} = \rho g \partial_x s - \partial_x \tau_{yy} - \partial_x \int_z^s \partial_y \tau_{yz}\, dz, \tag{A3}$$

where

$$\partial_x \tau_{yy} = \frac{9 w_a z h^{-5/2} \partial_x h \sqrt{\rho_w E g}}{\sqrt{3(1-\mu^2)}} e^{-\lambda y} \Big[\sin(\lambda y) + (\lambda y - 1)\cos(\lambda y) \Big], \tag{A4}$$

$$\partial_x \int_z^h \partial_y \tau_{yz}\, dz = -\frac{3}{4} \rho_w g w_a \partial_x h (h-2z) h^{-4} e^{-\lambda y} \Big(2\zeta \big[\sin(\lambda y) + \cos(\lambda y) \big] + \lambda y \big[h^2 - \zeta \big] \sin(\lambda y) \Big) \tag{A5}$$

and $\zeta = z(h+2z)$. Note that the x dependence of Eq. A2 is through the ice thickness h, which also appears in the expression for λ (Eq. 6). Integrating from the surface to the bed and dividing by ice thickness yields the depth averaged across-flow gradient in horizontal shear stress:

$$\partial_y \overline{\tau_{xy}} = \rho g \partial_x s - \frac{1}{h} \int_b^s \partial_x \int_z^s \partial_y \tau_{xy} dz. \tag{A6}$$

With the boundary condition that $\overline{\tau_{xy}}$ is zero at the centerline, we can integrate along y to give an expression for depth averaged horizontal shear stress, which is

$$\overline{\tau_{xy}} = \rho g h \partial_x s - \frac{3 \rho_w g w_a \partial_x h e^{-\lambda y} \lambda y \sin(\lambda y)}{4h}. \tag{A7}$$

It turns out that the second term on the R.H.S. of Eq. A7 is much smaller than the other two for any sensible choice in parameters and so the horizontal shear stress is balanced by the driving stress term to a very good approximation. Since the geometry along the x direction does not change with time the only temporal variation in τ_{xy} enters through the smaller second term. As such, $\dot{\tau}_{xy} \approx 0$; a curious finding given the large changes in centerline velocity but one that is borne out by examination of the stresses in our full-Stokes model (Sect. 6).

For a comparison with the idealised system of equations presented above, we take a 2-D slice through the ice shelf in the full-Stokes model (presented in Sect. 4) and look at the deviatoric stresses. We take this slice far away from the GL at $x = 0$ to avoid the additional bending stresses in this region. The lateral shear stress τ_{xy} is found to vary linearly from zero at the medial line to ~70kPa at the margin and is approximately constant with depth (see also Fig 6). Maximum variation in τ_{xy} over a tidal cycle is ~3%, despite the ice velocity doubling at the medial line. This matches closely with the profile predicted by Eq A7 using parameters taken from the model. The main discrepancy in stresses between the full-Stokes model and the simplified system of Eq. 2a is that modelled τ_{xx} becomes relatively large near the medial line, however since this is not the case near the margins, where most of the lateral shearing takes place, the approximation appears to not be a bad one.

The Cryosphere Discuss., https://doi.org/10.5194/tc-2017-193
Manuscript under review for journal The Cryosphere
Discussion started: 18 October 2017

Appendix B: Analytical solution for double clamped elastic beam

Much of the work on tidal bending of floating ice is based on beam theory, specifically the analysis of elastic beams on elastic foundations first explored by Hetenyi (1946). The classical solution for bending of a floating ice tongue was first derived by Robin (1958) and has since been used extensively in studies of ice flexural process (Holdsworth, 1969, 1977; Lingle et al., 1981; Stephenson, 1984; Vaughan, 1995; Smith, 1991; Hulbe et al., 2016; Sykes et al., 2009; Rignot, 1998). We will call this set of equations the long beam model (LBM). The set of boundary conditions (BCs) chosen in the LBM are as follows:

$$\left.\begin{matrix} w = 0 \\ w' = 0 \end{matrix}\right\} y = 0 \qquad \left.\begin{matrix} w = w_a \\ w' = 0 \end{matrix}\right\} y \to \infty \tag{B1}$$

where $w(y)$ is the vertical deflection of the neutral axis and w_a is the change in sea level due to tides. The assumption in Eq. B1 that ice is freely floating at the far-field boundary is valid in many circumstances, however the shelf downstream of RIS is only $\sim 30\,\mathrm{km}$ wide and so this set of BCs might not be appropriate. A better set of BCs for a narrow ice shelf consists of a beam clamped at both ends, such that

$$\left.\begin{matrix} w = 0 \\ w' = 0 \end{matrix}\right\} y = 0 \qquad \left.\begin{matrix} w = 0 \\ w' = 0 \end{matrix}\right\} y = 2W \tag{B2}$$

Starting from the beam equation for a floating ice shelf:

$$w^{IV}(y) = -\frac{12(1-\nu^2)}{Eh^3}\rho_w g(w_a(t) - w(y)), \tag{B3}$$

subject to the BCs in Eq. B2, we arrive at the solution:

$$w(y,t) = w_a(t)\left[1 - e^{-\lambda y}\left(C_1\sin(\lambda y) + C_2\cos(\lambda y)\right) + e^{\lambda y}\left(C_3\sin(\lambda y) + C_4\cos(\lambda y)\right)\right], \tag{B4}$$

where λ is given in Eq. 6 and the constants C_1 to C_4 are:

$$C_4 = \frac{1 - e^{2\lambda W}(\cos(2\lambda W) + \sin(2\lambda W))}{e^{4\lambda W} + 2e^{2\lambda W}\sin(2\lambda W) - 1} \tag{B5a}$$

$$C_2 = 1 + C_4 \tag{B5b}$$

$$C_3 = \frac{e^{2\lambda W}(\cos(2\lambda W) - \sin(2\lambda W)) - 1}{e^{4\lambda W} + 2e^{2\lambda W}\sin(2\lambda W) - 1} \tag{B5c}$$

$$C_1 = 1 + \frac{2\tan(2\lambda W)}{e^{4\lambda W}\tan(2\lambda W) + \tan(2\lambda W) + e^{4\lambda W} - 1} + C_4\left(\frac{e^{4\lambda W} + (3e^{4\lambda W} - 1)\tan(2\lambda W) - 1}{e^{4\lambda W} + (1 + e^{4\lambda W})\tan(2\lambda W) - 1}\right). \tag{B5d}$$

The Cryosphere Discuss., https://doi.org/10.5194/tc-2017-193
Manuscript under review for journal The Cryosphere
Discussion started: 18 October 2017

If the product λW is large (specifically, large in comparison to π) then the hinge zone is narrow compared to the ice shelf width. In this situation, $C_1 \approx C_2 \approx 1$ and $C_3 \approx C_4 \approx 0$, such that Eq. B4 reduces to the LBM solution (Robin, 1958). As it turns out, for the RIS where $W \approx$14 km, this turns out to be the case and so the simpler LBM differs only very slightly from the solution given in Eq. B4. As a result, we can safely use the LBM to approximate bending stresses on the RIS.

Acknowledgements. We are grateful to Rob Arthern, Brent Minchew and Teresa Kyrke-Smith for very helpful discussions. S. Rosier was funded by the UK Natural Environment Research Council large grant "Ice shelves in a warming world: Filchner Ice Shelf System" (NE/L013770/1).

The Cryosphere Discuss., https://doi.org/10.5194/tc-2017-193
Manuscript under review for journal The Cryosphere
Discussion started: 18 October 2017

References

Alley, S. A. R. B.: Tidal forcing of basal seismicity of ice stream C, West Antarctica, observed far inland, J.Geophys. Res., 102, 15,813–15,196, doi:10.1029/97JB01073, 1997.

Anandakrishnan, S., Voigt, D. E., and Alley, R. B.: Ice stream D flow speed is strongly modulated by the tide beneath the Ross Ice Shelf, Geophys. Res. Lett., 30, 1361, doi:DOI: 10.1029/2002GL016329, 2003.

Bindschadler, R. A., King, M. A., Alley, R. B., Anandakrishnan, S., and Padman, L.: Tidally controlled stick-slip discharge of a West Antasrctic ice stream, Science, 301, 1087–1089, doi:10.1126/science.1087231, 2003a.

Bindschadler, R. A., Vornberger, P. L., King, M. A., and Padman, L.: Tidally driven stickslip motion in the mouth of Whillans Ice Stream, Antarctica, Ann. Glaciol., 36, 263–272, doi:10.3189/172756403781816284, 2003b.

Brunt, K. M., King, M. A., Fricker, H. A., and Macayeal, D. R.: Flow of the Ross Ice Shelf , Antarctica , is modulated by the ocean tide, Journal of Glaciology, 56, 2005–2009, 2010.

Brunt, K. M., Fricker, H. A., and Padman, L.: Analysis of ice plains of the Filchner-Ronne Ice Shelf, Antarctica, using ICESat laser altimetry, Journal of Glaciology, 57, 965–975, n/a, 2011.

Christensen, R. M.: Theory of viscoelasticity, Academic Press 2nd Ed., New York, 1982.

Codiga, D. L.: Unified Tidal Analysis and Prediction Using the UTide Matlab Functions, Tech. rep., Graduate School of Oceanography, University of Rhode Island, Narragansett, RI., 2011.

Codiga, D. L. and Rear, L. V.: Observed tidal currents outside Block Island Sound: Offshore decay and effects of estuarine outflow, Journal of Geophysical Research: Oceans, 109, C07S05, doi:10.1029/2003JC001804, 2004.

Cuffey, K. M. and Paterson, W. S. B.: The physics of glaciers 4th ed., Elsevier, Amsterdam, 2010.

Doake, C., Corr, H. F. J., Nicholls, K. W., Gaffikin, A., Jenkins, A., Bertiger, W. I., and King, M. A.: Tide-induced lateral movement of Brunt Ice Shelf , Antarctica, Geophysical Research Letters, 29, 1–4, doi:10.1029/2001GL014606, 2002.

Gudmundsson, G. H.: Fortnightly variations in the flow velocity of Rutford Ice Stream, West Antarctica., Nature, 444, 1063–4, doi:doi:10.1038/nature05430, 2006.

Gudmundsson, G. H.: Tides and the flow of Rutford Ice Stream, West Antarctica, J. Geophys. Res., 112, F04 007, doi:10.1029/2006JF000731, 2007.

Gudmundsson, G. H.: Ice-stream response to ocean tides and the form of the basal sliding law, The Cryosphere, 5, 259–270, doi:10.5194/tc-5-259-2011, 2011.

Gudmundsson, G. H. and Jenkins, A.: Ice-flow velocities on Rutford Ice Stream, West Antarctica, are stable over decadal timescales, Journal of Glaciology, 55, 339–344, doi:10.3189/002214309788608697, 2009.

Gudmundsson, G. H., De Rydt, J., and Nagler, T.: Five decades of strong temporal variability in the flow of Brunt Ice Shelf, Antarctica, Journal of Glaciology, 63, 164–175, doi:10.1017/jog.2016.132, 2017.

Hetenyi, M.: Beams on elastic foundation, Ann Arbor, University of Michigan Press, 1946.

Holdsworth, G.: Flexure of a floating ice tongue, J. Glaciol., 8, 133–397, 1969.

Holdsworth, G.: Tidal interaction with ice shelves, Ann. Geophys., 33, 133–146, 1977.

Hulbe, C. L., Klinger, M., Masterson, M., Catania, G., Cruikshank, K., and Bugni, A.: Tidal bending and strand cracks at the Kamb Ice Stream grounding line, West Antarctica, Journal of Glaciology, 62, 816–824, doi:10.1017/jog.2016.74, 2016.

King, M. A., Makinson, K., and Gudmundsson, G. H.: Nonlinear interaction between ocean tides and the Larsen C Ice Shelf system, Geophysical Research Letters, 38, 1–5, doi:10.1029/2011GL046680, 2011.

Legresy, B., Wendt, A., Tabacco, I., Remy, F., and Dietrich, R.: Influence of tides and tidal current on Mertz Glacier, Antarctica, Journal of Glaciology, 50, 427–435, doi:10.3189/172756504781829828, 2004.

Lingle, C. S., Hughes, T. J., and Kollmeyer, R. C.: Tidal flexure of Jakobshavns Glacier, west Greenland, Journal of Geophysical Research: Solid Earth, 86, 3960–3968, doi:10.1029/JB086iB05p03960, 1981.

Makinson, K., King, M. A., Nicholls, K. W., and Gudmundsson, G. H.: Diurnal and semidiurnal tide-induced lateral movement of Ronne Ice Shelf, Antarctica, Geophysical Research Letters, 39, doi:10.1029/2012GL051636, 2012.

Marsh, O. J., Rack, W., Floricioiu, D., Golledge, N. R., and Lawson, W.: Tidally induced velocity variations of the Beardmore Glacier, Antarctica, and their representation in satellite measurements of ice velocity, The Cryosphere, 7, 1375–1384, doi:10.5194/tc-7-1375-2013, 2013.

Minchew, B. M., Simons, M., Riel, B., and Milillo, P.: Tidally induced variations in vertical and horizontal motion on Rutford Ice Stream, West Antarctica, inferred from remotely sensed observations, Journal of Geophysical Research: Earth Surface, pp. 1–24, doi:10.1002/2016JF003971, 2016.

Padman, L., Fricker, H. A., Coleman, R., Howard, S., and Erofeeva, S. Y.: A new tide model for the Antarctic ice shelves and seas, Ann. Glaciol., 34, 247–254, 2002.

Rignot, E. J.: Hinge-line migration of Petermann Gletscher, north Greenland, detected using satellite-radar interferometry, Journal of Glaciology, 44, 469–476, 1998.

Robin, G. d. Q.: Seismic shooting and related investigations, Norwegian-British-Swedish Antarctic Expedition 1949-1952, 5, 122–125, 1958.

Rosier, S. H. R. and Gudmundsson, G. H.: Tidal controls on the flow of ice streams, Geophysical Research Letters, 43, 4433–4440, doi:10.1002/2016GL068220, 2016GL068220, 2016.

Rosier, S. H. R., Gudmundsson, G. H., and Green, J. A. M.: Insights into ice stream dynamics through modeling their response to tidal forcing, The Cryosphere, 8, 1763–1775, doi:10.5194/tc-8-1763-2014, 2014.

Rosier, S. H. R., Gudmundsson, G. H., and Green, J. A. M.: Temporal variations in the flow of a large Antarctic ice-stream controlled by tidally induced changes in the subglacial water system, The Cryosphere Discussions, 9, 1–33, doi:10.5194/tcd-9-1-2015, 2015.

Rosier, S. H. R., Gudmundsson, G. H., King, M. A., Nicholls, K. W., Makinson, K., and Corr, H. F. J.: Strong tidal variations in ice flow observed across the entire Ronne Ice Shelf and adjoining ice streams, Earth System Science Data Discussions, 70, doi:10.5194/essd-2017-70, 2017.

Sergienko, O. V., Macayeal, D. R., and Bindschadler, R. A.: Stick–slip behavior of ice streams: modeling investigations, Annals of Glaciology, 50, 87–94, doi:10.3189172756409789624274, 2009.

Smith, A. M.: The use of tiltmeters to study the dynamics of Antarctic ice-shelf grounding lines, J. Glaciol., 37, 51–58, 1991.

Stephenson, S. N.: Glacier flexure and the position of grounding lines: Measurements by tiltmeter on Rutford Ice Stream Antarctica, Ann. Glaciol., 5, 165–169, 1984.

Sykes, H. J., Murray, T., and Luckman, A.: The location of the grounding zone of Evans Ice Stream, Antarctica, investigated using SAR interferometry and modelling, Annals of Glaciology, 50, 35–40, doi:doi:10.3189/172756409789624292, 2009.

Thompson, J., Simons, M., and Tsai, V. C.: Modeling the elastic transmission of tidal stresses to great distances inland in channelized ice streams, The Cryosphere Discussions, 8, 2119–2177, doi:10.5194/tc-8-2007-2014, 2014.

Vaughan, D. G.: Tidal flexure at ice shelf margins, J. Geophys. Res., 100, 6213–6224, 1995.

Walker, R. T., Christianson, K., Parizek, B. R., Anandakrishnan, S., and Alley, R. B.: A viscoelastic flowline model applied to tidal forcing of Bindschadler Ice Stream, West Antarctica, Earth and Planetary Science Letters, 319–320, 128 – 132, doi:http://dx.doi.org/10.1016/j.epsl.2011.12.019, 2012.

Walker, R. T., Parizek, B. R., Alley, R. B., and Nowicki, S. M. J.: A Viscoelastic Model of Ice Stream Flow with Application to Stick-Slip Motion, Frontiers in Earth Science, 4, 2, doi:10.3389/feart.2016.00002, 2016.